Leadership in Sustainable Infrastructure
Leadership en Infrastructures Durables

Vancouver, Canada
May 31 – June 3, 2017/ *Mai 31 – Juin 3, 2017*

DESIGN AND PERFORMANCE EVALUATION OF SHAPE MEMORY ALLOY (SMA) CROSS-WIRE CONFIGURED HIGH DAMPING RUBBER BEARING

Spencer, Kaila[1,4], Hedayati Dezfuli, Farshad[2], Alam, M. Shahria[3]

[1,2,3] University of British Columbia, Canada
[4] kailaspencer12345@gmail.com

Abstract: Base Isolation systems are currently one of the common methods used to maintain the general integrity of bridges and other structures from the damages caused by seismic activity. The use of these isolators can come with some complications due to their limitations with regards to aging as well as possible deformation or failure after experiencing a substantial earthquake; this results in the need to constantly maintain or replace the isolators, which can be costly and time consuming. The use of shape memory alloy (SMA) wires in high damping rubber bearings (HDRBs) helps to resolve most of the major problems associated with the commonly used isolation devices, which would allow the isolation devices to possibly experience seismic events without needing to be consistently fixed or replaced. This study evaluates the design of a new smart elastomeric isolator, called SMA-HDRB, using a cross configuration for the wires, as well as different material types of SMAs, and pre-straining effect. The hysteretic shear behavior of designed SMA-HDRBs with the cross configuration shows that the lateral flexibility and residual deformation are reduced compared to normal HDRBs. Results also demonstrate that pre-straining the wires helps to prevent the reduction of the lateral flexibility; and increasing the diameter of the wires increases the effective horizontal stiffness and total energy dissipation capacity of the base isolation system.

1 INTRODUCTION

In seismic prone areas, many buildings experience deflections due to large earthquakes. To reduce the effect of these deflections on the structure there are many different techniques in place; seismic isolation is one of the most commonly used techniques to protect bridges from extreme damage due to these earthquake events. There are various types of isolators that have been developed, tested, and are currently being used to effectively help reduce the effects of seismic activity on buildings such as lead-rubber bearings, high damping rubber bearings, friction-pendulum bearings, magneto-rheological damper, and steel plate damper (Ghobarah and Ali, 1990. Warn and Whittaker, 2004. Bhuiyan et al. 2009). Lead rubber bearings (LRB) and the high damping rubber bearing (HDRB) are the two most popular isolation devices. These devices are known to have high damping properties, which allows them to adequately reduce the deflections caused by earthquakes. Due to the nature of the devices, many of them are prone to issues caused by aging and durability limitations, maintenance, temperature-sensitive performance, and needing to be properly realigned after an earthquake. A way to reduce the number of issues with current HDRB devices is to incorporate superelastic shape memory alloys (SMA) into the design of the isolators. Superelastic SMA can experience large deformations and return to its original shape and position after a large scale seismic event; so, it can potentially recover its inelastic deformation after an earthquake. Superelastic SMA is an ideal material to be used in isolation systems due to their flag-shaped hysteresis curve, its ability to recover after large strain and deformation, long endurance, and resistance to corrosion. Hedayati Dezfuli and Alam investigated the performance of Natural Rubber Bearings (NRBs) when SMAs are incorporated and concluded that using SMA wires can be beneficial to NRBs in terms of energy

dissipation capacity and re-centering capability (Hedayati Dezfuli and Alam, 2013). Therefore, it would be advantageous to evaluate the effect of SMA wires on the response of HDRBs, and whether it would be beneficial to consider implementing SMA materials into the design of elastomeric isolators.

In this study, a cross wire configuration for SMA wires is considered; the effect of the wires on the HDRB is assessed, and the performance of SMA-HDRB is compared to that of the regular HDRB. A performance-based design approach is also presented to determine the pre-strain and the radius of cross-section of SMA wires. To assess the performance of the SMA-HDRBs on a structure under seismic loadings, a three-span continuous steel girder concrete-reinforced pier supported bridge is modeled, and dynamic time history analyses are performed. The total energy dissipated by rubber bearings, the relative lateral displacement in rubber bearings, and the maximum acceleration of the bridge deck for non-isolated (fixed-base) and isolated bridges are determined.

2 SMA INCORPORATED ELASTOMERIC ISOLATORS

SMA-based smart rubber bearings are advantageous when they come to stability, re-centering capability, high energy dissipation capacity and long service life. They alleviate the seismic response of structures in terms of deflection of the structure, internal forces, acceleration, and have superior performance in terms of fatigue property and energy dissipation capacity compared to conventional rubber bearings (Suduo and Xiongyan, 2007). In this study, the elastomeric isolator consists of high damping rubber layers bonded to carbon fiber-reinforced polymer (CFRP) composite plates. The aspect ratio (R) of bearing, defined as the height to the length of laminated pad, is equal to 0.36. The geometric properties of the bearing are listed in Table 1. The thickness of the steel, elastomer, and carbon fibre-reinforced polymer layers are given as t_s, t_e, t_f, respectively.

Table 1: Geometric properties of CFR-HDRB, including the length and radius of SMA wires

Elastomeric Bearing								SMA Wire	
L (mm)	W (mm)	H (mm)	t_s (mm)	t_e (mm)	t_f (mm)	n_e	n_f	L_{SMA} (mm)	r_{SMA} (mm)
250	250	120	15	4.71	0.31	18	17	2352.9	2.5

In the proposed cross-wire configuration, two continuous SMA wires, made of an FeNiCoAlTaB alloy, are wound around the rubber bearing diagonally as shown in Figure 1. The wires are passed through steel hooks connected to the corners of the steel supporting plates. Four hooks are welded to the bottom surface of the top supporting plate, and another four to the top surface of the bottom supporting plate.

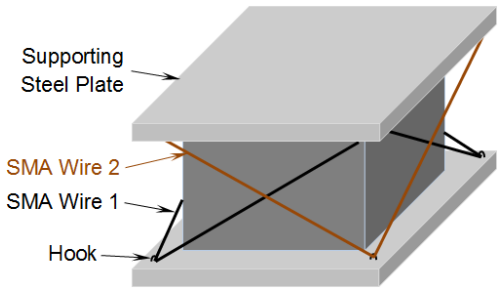

Figure 1: Smart rubber bearing with cross SMA wires

Knowing the fact that the superelastic effect of SMA occurs at temperatures above the austenite finish temperature, T_f^A, the temperature at which SMA wires are functional in base isolation applications should be higher than T_f^A. Since the minimum ambient temperature in countries with cold climatic conditions may go below -20°C, the austenite finish temperature of SMA wires should be lower than this temperature. The chosen ferrous SMA (FeNiCoAlTaB) has a superelastic strain of about 13.5%, an austenite elastic modulus of 46.9 GPa, and an austenite finish temperature of -62°C (Tanaka et al., 2010).

3 FINITE ELEMENT MODELING

3.1 High Damping Rubber Bearing

In the finite element method (FEM), element SOLID185 is selected to be used for both reinforcement and elastomeric layers. Stress stiffening, large deflection, and large strain can be modeled using SOLID185. The steel shim used in HDRB is modeled as an isotropic material with a Young's modulus of 210 GPa and a Poisson's ratio of 0.3. Many studies showed that although the hyperelastic material model can simulate the response of natural low damping rubber, this model does not accurately capture the behavior of high damping rubber materials (Bhuiyan et al. 2009, Yoshida et al. 2004, Amin et al. 2006). The hyper-viscoelastic model could correctly simulate the highly nonlinear behavior of high damping rubber under cyclic lateral displacements (Hedayati Dezfuli and Alam 2013, Hedayati Dezfuli and Alam 2013). Here, Mooney-Rivlin hyperelastic model is combined with Prony viscoelastic model to replicate the behavior of high damping rubber (Hedayati Dezfuli and Alam 2012). The material properties of the carbon fiber-reinforced sheets (carbon/epoxy), which perform as an orthotropic material, as well as material constants of the hyper-viscoelastic model used for high damping rubber (HDR) are listed in Table 2.

Table 2: Material properties of FRP composite (Howie and Karbhari 1994) and material constants of hyper-viscoelastic model

FRP Composite (Carbon/Epoxy)				HDR	
Elastic Modulus (MPa)	Shear Modulus (MPa)	Poisson's Ratio	Tensile Strength (MPa)	Mooney-Rivlin	Prony
E_x=73300.0	G_{xy}=1761.0	v_{xy}=0.310	755.0	C_{10} =1.192	a_1=0.765
E_y=4613.8	G_{yz}=1659.5	v_{yz}=0.390		C_{01}=0.547	t_1=0.124
E_z =4613.8	G_{zx}=1761.0	v_{zx}=0.019		C_{11}=-0.038	a_1=0.061
				C_{02}=0.047	t_2=65.82
				C_{20}=0.108	
				C_{12}=0.000	
				C_{21}=-0.013	
				C_{03}=0.000	
				C_{30}=0.002	

To validate the FE model, the hysteretic shear response of a HDRB consisting of two elastomer layers, each with a thickness of 5 mm, is compared with experimental tests conducted by Dall'Asta and Ragni (Dall'Asta and Ragni, 2006). The test was performed under pure cyclic loadings (no vertical pressure) at 43%, 90%, 155%, and 200% shear strain amplitudes amplitude, and a frequency of 0.49 Hz. The results retrieved from the finite element simulation (see Figure 2) are similar to the experimental tests. The maximum difference between the numerical and experimental results in the horizontal stiffness is 5%, which happens at 200% shear strain. Both experimental and numerical results show that the maximum horizontal loads experienced at 43%, 90%, 155%, and 200% shear strains are 34 kN, 51 kN, 71 kN, and 85 kN, respectively.

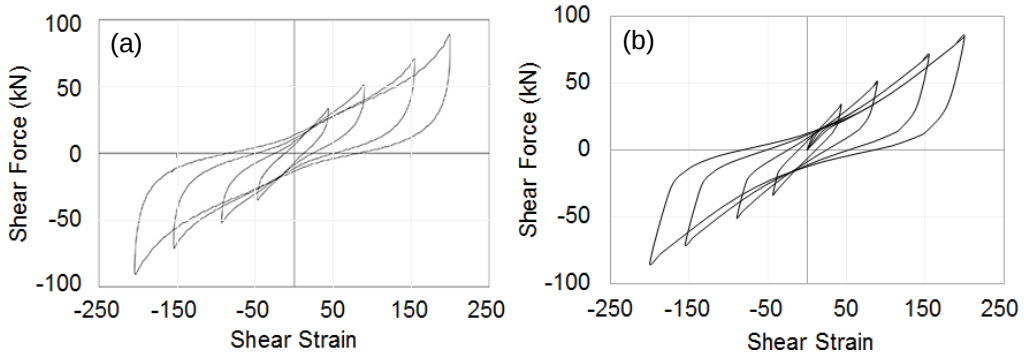

Figure 2: Hysteresis of HDRB at 43%, 90%, 155%, and 200% shear strains; (a) experimental results (adapted from (Dall'Asta and Ragni, 2006)), (b) finite element simulations

3.2 SMA Wire-based High Damping Rubber Bearing

In generating the FE model of the SMA wire-based high damping rubber bearing (SMA-HDRB), a method of superposition is implemented by decoupling the rubber bearing and SMA wires. While the frictional force generated between the wire and the hook may change the characteristics and accordingly, the response of SMA wires, there is smooth contact assumed for generating the FE model. The friction can be minimized by reducing the contact between the hook and SMA wire.

In this study, exerted forces to the elastomeric isolator due to SMA wires are considered instead of modelling the steel hooks and their contact with the wires. This assumption substantially reduces the complexity of the finite element simulation. Assuming the effects of torsion, rotation about all axes, delamination due to the shear deformation in laminated pad, and vibration in the vertical direction are ignored, the formula of SMA strain is provided in a simplified case (i.e. strain induced by a displacement in the x direction, as shown in Figure 3). The effect of vertical displacement due a constant compressive load is assumed to be negligible on the SMA strain since the vertical deflection is very small compared to the lateral displacement.

$$\varepsilon_{SMA} = \frac{L_{SMA} - L_{0\,SMA}}{L_{0\,SMA}};$$

[1]

$$L_{0\,SMA} = 2\left(\sqrt{(L+2l_e)^2 + H_{eff}^2} + \sqrt{(W+2w_e)^2 + H_{eff}^2}\right)$$

$$L_{SMA} = \sqrt{(L+2l_e+\Delta X)^2 + H_{eff}^2} + \sqrt{(L+2l_e-\Delta X)^2 + H_{eff}^2} + 2\sqrt{\Delta X^2 + (W+2w_e)^2 + H_{eff}^2}$$

In this equation, the initial length, L_0, remains constant while, length L changes over the time as it is a function of displacement, ΔX. Considering an square shape for the HDRB (i.e. equal lengths in the x and y directions), W is equal to L, and w_e is equal l_e.

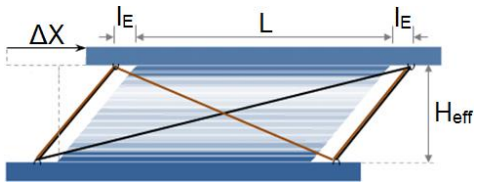

Figure 3: SMA-HDRB with cross wire configuration subject to displacement in x direction

The axial stress in SMA wires can be determined from the stress-strain relationship of shape memory alloys (Aurichhio, 2001). Using the value of the axial stress and the direction of wires at each time step, the force vectors exerted from the SMA wire to the HDRB are computed. The equivalent forces are applied to the rubber bearing at each time step while running the nonlinear analysis.

4 SEISMIC PERFORMANCE OF SMA-HDRB

The purpose of the base isolation system is to reduce the acceleration of the deck, and thus, the force transferred to the piers of the bridge. A scaled three-span continuous steel girder bridge is modeled and analyzed using finite element software Seismostruct in order to evaluate the performance of the SMA-HDRB under seismic loadings (SeismoStruct, 2012). In this regard, time history analyses are performed for three earthquake records: Loma Prieta, Northridge, and Kobe with the maximum peak ground acceleration of 0.46g, 0.38g, and 0.42g, respectively. The magnitude of the ground motions in the Richter scale is between 6.7 and 7.0. Since it is assumed that the bridge is located in Vancouver city, all ground motion records are scaled by Vancouver design response spectrum with a damping ratio of 5% as a design ground motion level. The earthquake records are scaled using SeismoMatch software in which the target spectrum (i.e. Vancouver response spectrum) is considered in a range of periods of 0 to 4 seconds. The bridge is comprised of continuous RC deck-steel girder isolated by four rubber bearings installed between the steel girder and pier caps. The details of the structure (geometry and material properties) of the bridge can be

found in (Hedayati Dezfuli and Alam, 2013). The details of the analytical model can also be found in (Alam et al., 2012).

To determine if the performance of the SMA-HDRB is superior than regular HDRBs, the seismic responses of bridges isolated with SMA-HDRB and HDRB are compared. HDRBs and SMA-HDRBs are modeled as link elements using bilinear kinematic hardening model with three characteristics: initial stiffness (K_0), yield force (F_Y), and post-yield hardening ratio (r) defined in the longitudinal and transverse directions. Here, the behavior of rubber bearing is idealized using symmetric bilinear hysteresis curve as an approximation.

5 RESULTS AND DISCUSSION

5.1 Design of SMA-HDRB

The relatively large amount of yield stress, defined as the stress at which the forward phase transformation (austenite to martensite) starts, exerts a large lateral force to the rubber bearing in the opposite direction of the cyclic horizontal displacement. As a result of this lateral force, the effective horizontal stiffness is significantly increased compared to the HDRB. In order to lessen this negative effect, the SMA wire should be pre-strained before being used as a damper in the rubber bearing (Choi et al., 2005). In the pre-strained wires, the forward phase transformation occurs at a lower strain level and consequently, the yield stress decreases.

The effective horizontal stiffness and the total energy dissipation capacity of the base isolation system can be increased by increasing the diameter of the SMA wires. However, increasing the amount of pre-strain decreases the horizontal stiffness in the wires. Since it is beneficial to simultaneously increase the lateral flexibility and maximize the damping capacity of the rubber bearing, it is more advantageous to change both the diameter and pre-strain of SMA wires for the sake of reaching the target horizontal stiffness, rather than just altering the diameter of wires. The flow chart of the design procedure is shown in Figure 4.

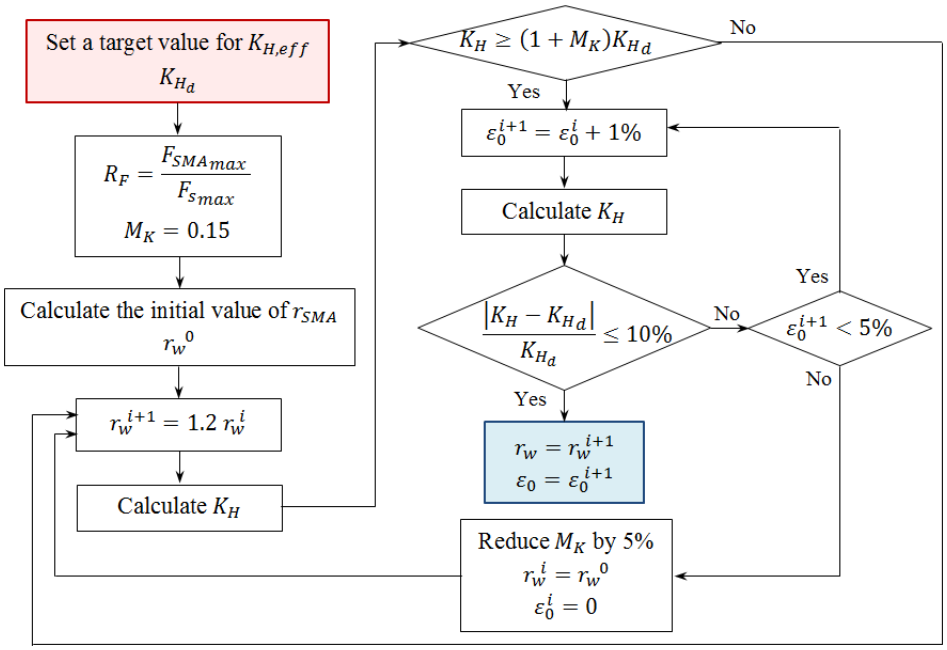

Figure 4: Design procedure to determine the diameter and pre-strain of SMA wires

In this design procedure, a target value for the effective horizontal stiffness ($K_{H\,d}$) of the elastomeric isolator is set before determining the required diameter and pre-strain of the wires. Then, depending on the size of the isolator, the diameter of SMA wires increases, starting from an initial value. Based on the geometry of rubber bearing and the configuration of SMA wires, a minimum initial diameter r^0_w is obtained from a force ratio (R_F). This parameter is defined as a ratio of the maximum lateral force generated by SMA wires (F_{SMA}

$_{max}$) to the maximum shear force of the regular bearing (i.e. bearing without SMA) ($F_{s\ max}$) at 100% shear strain. The force ratio is set to a value at which the effect of the SMA wires can be observed on the hysteresis curve of the isolator (here considered 10%). Knowing the maximum strain in the SMA wire at 100% shear strain, from Eq. (1), and thus, the maximum axial stress in the wire, the initial radius of SMA wire, r^0_w, can be obtained from $F_{SMA\ max}$ calculated using the force ratio. The stiffness margin, M_K (having an initially considered value of 15%), is defined to determine the relative difference between the calculated effective lateral stiffness of SMA-HDRB, K_H, and the target value of stiffness, $K_{H\,d}$. Under this condition, the radius of wires should increase up to a level at which K_H is 15% higher than the target value. The pre-strain in the wires increases and the effective lateral stiffness can be calculated by fixing the radius of the SMA wires. Considering pre-strain values lower than 5%, if the reduction in shear force due to pre-straining the SMA wires causes the lateral stiffness to be reduced and reaches the target point, with a 10% error, the values of radius and pre-strain are selected and the design procedure is finished. Otherwise, the stiffness ratio decreases by 5%, the radius of wire and the pre-strain are set to their initial values (r^0_w and 0, respectively), and then, the effective horizontal stiffness is recalculated. Based on the described design procedure, the radius of SMA wires increases from an initial value of 1 mm to 2.5 mm. Going above the recommended wire diameter will reduce the wires effectiveness as they will not be able to take the deflections as well as is required in order for them to be beneficial.

To allow the SMA wires to operate as required, it is important to have use continuous wires in the design. In order to have a continuous wire wrapped around the bearing, both ends of the wire are attached using a wire joiner. As shown in Figure 5, wires are rotated around a bolt and fixed inside of a hollow cylinder made of aluminum. In this proposed system, a certain level of pre-strain can be applied to the wires by rotating the bolt and then, fixing it using the nut.

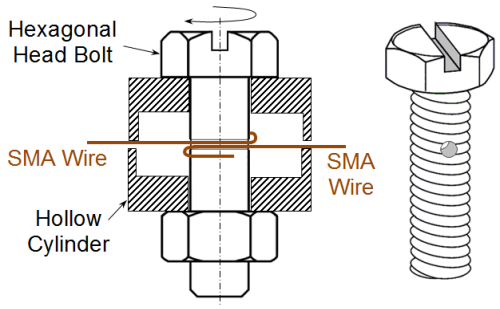

Figure 5: Wire joiner for fixing the SMA wire and applying pre-strain

5.2 Hysteretic Behavior of HDRB and SMA-HDRB

In order to observe the behavior of the SMA-HDRB compared to normal HDRBs, numerical finite element simulations were performed on the bearings at different shear strain levels. Figure 6 depicts the resulting lateral force-deflection curves of the HDRB and SMA-HDRB during these tests. The SMA wires used in the design of the SMA-HDRB has a cross sectional area of 19.6 mm^2. In the cross configuration, for shear strains up to 150%, the maximum strain induced in the SMA wires is 4.99% which is lower than the superelastic strain range of FeNiCoAlTaB.

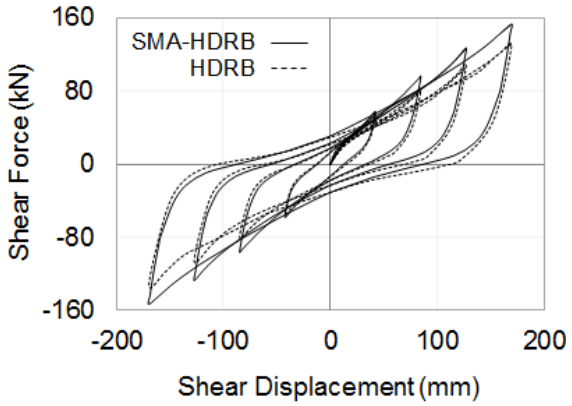

Figure 6: Hysteresis curves of HDRB and SMA-HDRB at γ = 50%, 100%, 150%, and 200%

The maximum lateral force in the SMA-HDRB at 200% shear strain is 153 kN. After finishing the forward phase transformation in SMA wires, at strain levels above 15%, the stress increases rapidly with a rate equal to the martensitic modulus of elasticity. As a result, a huge amount of stress is generated in SMA wires when the strain reaches 27.5%, and consequently, the lateral stiffness of the base isolator considerably increases. Table 3 compares the characteristics of HDRB and SMA-HDRB for different shear strain amplitudes. At γ = 50%, the effective horizontal stiffness of HDRB increases by 4% when cross wires are used. At γ = 200%, the effective horizontal stiffness of SMA-HDRB is 16% greater than that of HDRB, while the residual deformation decreases by 22%. Another finding is that the cross SMA wires causes a maximum reduction of 32% in the residual deformation HDRB.

Table 3: Effective horizontal stiffness and residual deformation of HDRB and SMA-HDRB

	HDRB		SMA-HDRB			
γ (%)	K_H (kN/mm)	R.D. (mm)	K_H (kN/mm)	Δ_{KH} (%)	R.D. (mm)	Δ_{RD} (%)
50	1.30	14.9	1.36	4	12.4	-17
100	0.96	36.4	1.14	18	33.0	-9
150	0.85	69.2	1.00	18	54.9	-21
200	0.78	109.4	0.90	16	86.6	-22

5.3 Dynamic Time History Analysis

The acceleration of the bridge deck, the relative lateral displacement of rubber bearings, and the total energy dissipated by elastomeric isolators are calculated for two cases where HDRB and SMA-HDRB are implemented. Three earthquake records: Loma Prieta, Northridge, and Kobe are scaled by Vancouver design response spectrum (with a 5% damping ratio) and considered in time history analyses.

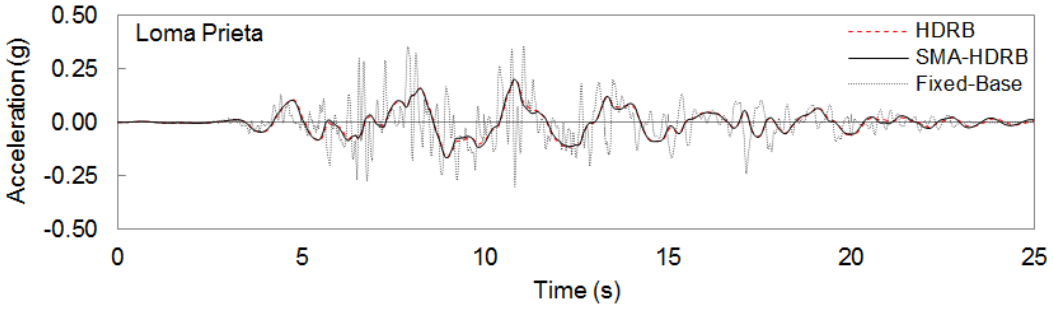

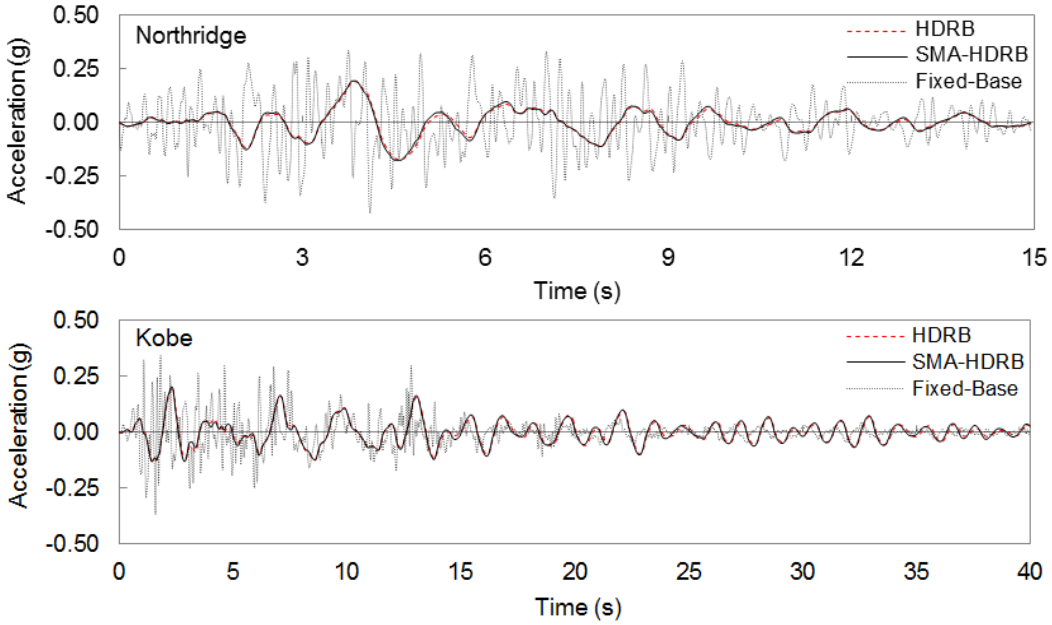

Figure 7: Time variation of deck acceleration for fixed-base and isolated bridges

Figure 7 depicts variations of the deck acceleration for non-isolated and isolated bridges subjected to three considered ground motions. It is observed that implementing rubber bearings into the bridge causes a significant reduction in the acceleration of the deck when HDRB and SMA-HDRB are used. To provide a detailed comparison between performances of HDRB and SMA-HDRB, the peak deck accelerations of the non-isolated and isolated bridges are given in Table 4.

Table 4: Peak deck acceleration, peak shear strain, and total energy dissipation capacity of HDRB and SMA-HDRB

	Loma Prieta			Northridge			Kobe		
	A_{max} (g)	γ_{max} (%)	U (kJ)	A_{max} (g)	γ_{max} (%)	U (kJ)	A_{max} (g)	γ_{max} (%)	U (kJ)
Fixed-base Bridge	0.36	-	-	0.42	-	-	0.35	-	-
HDRB	0.20 (45%)*	120%	88.9	0.19 (55%)	119%	81.9	0.20 (45%)	124%	161.0
SMA-HDRB	0.20 (44%)	115% (-4%)	95.3 (7%)	0.19 (54%)	113% (-5%)	95.7 (17%)	0.20 (44%)	118% (-5%)	178.5 (11%)

* Relative difference

Under Loma Prieta, HDRB and SMA-HDRB decrease the maximum deck acceleration to 0.20g which is about 45% lower than the maximum peak deck acceleration in the non-isolated bridge. When the bridge is subjected to Northridge earthquake, HDRB and SMA-HDRB diminish the maximum peak deck acceleration by 55% and 54%, respectively. In Kobe earthquake, equipping the bridge by HDRB and SMA-HDRB leads to about 45% and 44% decrease in the maximum peak deck acceleration, respectively. This results show that implementing cross SMA wires into HDRBs has negligible effect on the peak acceleration of bridge deck.

Time variation of the lateral displacement of HDRB and SMA-HDRB under three earthquakes is plotted in Figure 8, and the peak shear strains in the rubber bearings are listed in Table 4.

Rubber bearings laterally isolate the deck from the pier and as a result, when the deck undergoes a large deflection, the base shear force noticeably decreases due to the reduction in the deck acceleration. Results show that under Loma Prieta earthquake, by using HDRB or SMA-HDRB, shear strain does not exceed 120%. Under Northridge and Kobe earthquake records, the maximum lateral deflection of HDRB and SMA-

HDRB does not go beyond the 125% and 120% of the total thickness of rubber layers, respectively. Such behaviors prove that using SMA wires can control the shear deformation and restrict the lateral flexibility of the rubber bearings.

The total energy dissipated by HDRB and SMA-HDBR during Loma Prieta, Northridge, and Kobe ground motions is listed in Table 4. Under Kobe ground motion, HDRB has an energy dissipation capacity of 161 kJ, while SMA-HDRB dissipates 179 kJ energy (11% more). When the bridge is excited by Northridge earthquake, the total energy dissipation capacity of SMA-HDRB is 17% higher than that of HDRB. These findings reveal that SMA-HDRB has a higher capability in dissipating the seismic energy compared to HDRB because of the flag-shaped hysteresis of SMA wires.

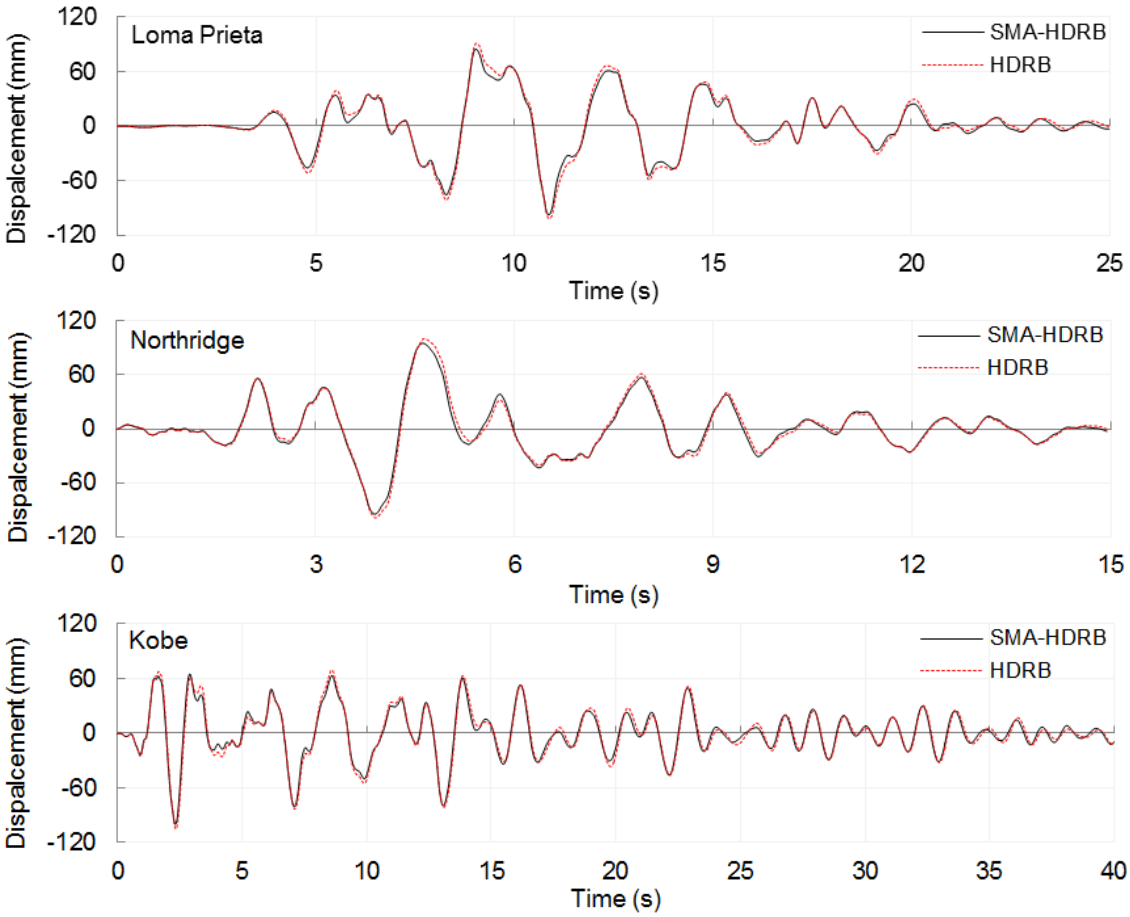

Figure 8: Time variation of lateral displacement of HDRB and SMA-HDRB

6 CONCLUSIONS AND RECOMMENDATION

The main purposes of implementing SMA wires in rubber bearings are to improve the re-centering capability and the energy dissipation capacity of the base isolator. SMA wires can effectively improve these two characteristics for natural rubber bearings (Hedayati Dezfuli and Alam, 2013). However, findings of this study show that applying SMA wires to HDRBs is not efficient in terms of reducing the residual deformation. This fact implies that SMA wires do not considerably affect the re-centering capability of the HDRBs. Though, the influence of SMA wires on the energy dissipation capacity of HDRBs is significant. Results obtained from dynamic time history analyses performed on the three-span continuous bridge also demonstrate that SMA wires can noticeably improve the energy dissipation capacity of HDRBs. Overall, it can be concluded that implementing cross SMA wires into HDRBs can improve the performance of bearings in controlling and regulating the seismic response of the bridge structure. However, in terms of deck acceleration reduction, performances of HDRB and SMA-HDRB are almost the same.

Considering the marginal improvement in the performance (i.e. self-centering and energy dissipation capacity) of HDRBs using SMA wires reveals that Nickel-Titanium-based wires cannot be good candidates for HDRBs due to their high cost. However, the application of ferrous SMAs (e.g. FeNiCoAlTaB), which is more cost-effective than NiTi wires, can be further studied and approved.

While SMAs are still relatively expensive, an important point is that increasing use of SMAs in civil infrastructures will potentially reduce the cost of SMAs due to larger supply and demand, as has been observed for other materials such as fiber reinforced polymers in the construction industry. In order to come up with an optimized case, both cost and efficiency of SMA wires should be taken into account by defining a multi-criteria decision making problem in which the cost is minimized and the strain of SMA wires is maximized.

ACKNOWLEDGEMENTS

The financial contribution of Natural Sciences and Engineering Research Council of Canada (NSERC) through Discovery Grant was critical to conduct this research and has been gratefully acknowledged.

REFERENCES

Alam, M.S., Bhuiyan, MAR. and Billah, AHMM. 2012. Seismic fragility assessment of SMA-bar restrained multi-span continuous highway bridge isolated by different laminated rubber bearings in medium to strong seismic risk zones. *Bulletin of Earthquake Engineering*; 10(6):1885-1909.

Amin, AFMS., Lion, A., Sekita, S. and Okui, Y. 2006. Nonlinear dependence of viscosity in modeling the rate-dependent response of natural and high damping rubbers in compression and shear: experimental identification and numerical verification. *International Journal of Plasticity*; 22(9):1610-1657.

Auricchio, F. 2001. A robust integration-algorithm for a finite-strain shape-memory-alloy. *International Journal of Plasticity*; 17(7): 971-990.

Bhuiyan, AR., Okui, Y., Mitamura, H. and Imai, T. 2009. A rheology model of high damping rubber bearings for seismic analysis: identification of nonlinear viscosity. *International Journal of Solids and Structures*; 46(7-8):1778-1792.

Choi, E., Nam, TH. and Cho, BS. 2005. A new concept of isolation bearings for highway steel bridges using shape memory alloys. *Canadian Journal of Civil Engineering*; 32(5):957-967.

Dall'Asta, A. and Ragni, L. 2006. Experimental tests and analytical model of high damping rubber dissipating devices. *Engineering Structures*; 28(13):1874-1884.

Ghobarah, A. and Ali, HM. 1990. Seismic design of base-isolated highway bridges utilizing lead-rubber bearings. *Canadian Journal of Civil Engineering*; 17(3):413-422.

Hedayati Dezfuli, F. and Alam, MS. Material modeling of high damping rubber in finite element method. In Proceedings of 3rd *International Structural Specialty Conference*, Edmonton, Alberta, Canada, 6-9 June 2012.

Hedayati Dezfuli, F. and Alam, MS. 2013. Multi-criteria optimization and seismic performance assessment of carbon FRP-based elastomeric isolator. *Engineering Structures*; 49: 525-540.

Hedayati Dezfuli, F. and Alam, MS. 2013. Shape memory alloy wire-based smart natural rubber bearing. *Smart Materials and Structures*; 22(4) 045013.

Howie, I. and Karbhari, VM. 1994. Effect of materials architecture on strengthening efficiency of composite wraps for deteriorating columns in north-east. In proceedings of *3rd Materials Engineering Conference, Infrastructure: New Materials and Methods of Repair*, pp. 199-206.

SeismoStruct, 2012. SeismoStruct help file. Available from www.seismsoft.com.

Suduo, X. and Xiongyan, L. 2007. Control devices incorporated with shape memory alloy. *Earthquake Engineering and Engineering Vibration*; 6(2):159-169.

Tanaka, Y., Himuro, Y., Kainuma, R., Sutou, Y., Omori, T. and Ishida, K. 2010. Ferrous polycrystalline shape-memory alloy showing huge superelasticity. *Science*; 327(5972):1488-1490.

Warn, GP. and Whittaker, AS. 2004. Performance estimates in seismically isolated bridge structures. *Engineering Structures*; 26(9):1261-1278.

Yoshida, J. Abe, M. and Fujino, Y. 2004. Constitutive model of high-damping rubber materials. *Journal of Engineering Mechanics*, ASCE; 130(2):129-141.